06

Residual stresses at the interface between carrier tape and YSZ layer in manufacture of 2G HTS wires

© A.V. Irodova, E.A. Golovkova, O.A. Kondratiev, V.S. Kruglov, V.E. Krylov, S.A. Tikhomirov, S.V. Shavkin

National Research Center „Kurchatov Institute“,
123182 Moscow, Russia
e-mail: Irodova_AV@nrcki.ru

Received August 1, 2022
Revised August 1, 2022
Accepted August 23, 2022

Using X-ray diffraction, there were determined the residual stresses on the surface of the AISI 310S stainless steel carrier tape used in manufacture of the second generation high temperature superconducting (2G HTS) wires at the National Research Center „Kurchatov Institute“, from delivery to deposition of the main buffer layer YSZ between the tape and the superconducting layer, and the residual stress in the buffer layer YSZ itself. The compressive stress of -0.8 GPa induced by rolling was found on the surface of the tape as-delivered. During processing, it varies from -0.5 to -1.1 GPa. At each stage, its depth distribution was found down to $10\,\mu$m, and the residual stresses caused by processing were determined. The residual stress in the YSZ layer deposited using the ABAD technology is compressive and amounts to -3.29 GPa. The layer has a defective single-crystal structure in type to radiation swelling with the unstressed lattice period of 5.1820 Å, 0.9% larger than in ordinary crystal. The results obtained are in agreement with the data of the earlier neutron diffraction study of residual stresses inside the carrier tape.

Keywords: residual stress, 2G HTS wires, AISI 310S tape, YSZ layer, YSZ crystal structure, X-ray diffraction.

DOI: 10.21883/TP.2022.12.55196.197-22

Introduction

High-temperature superconducting wires of the second generation (HTS-2G wires) based on superconducting ceramics $RBa_2Cu_3O_{7-\delta}$, where R — rare earth metal (REBCO) or yttrium (YBCO), are recognized as non-alternative materials for creating powerful magnets for compact thermonuclear reactors, electric aircraft engines and generators, electrically driven space propulsion systems, shields protecting from space radiation, and much more [1]. When operating in strong magnetic fields, they must withstand the high tensile stresses that occur in the magnet windings without loss of current-carrying capacity.

HTS-2G wires have a complex multilayer architecture [1] with three basic components. The carrier metal tape-substrate, among other things, provides the mechanical strength of the wire. The almost single crystal superconducting layer REBCO (YBCO) determines the current-carrying characteristics of the wire. The highly textured buffer layers between the carrier tape and the superconductive layer serve to epitaxially grow the superconductive layer and to protect it from chemical interaction with the tape material. All other layers deposited on the superconducting layer perform protective and stabilizing functions. Processing methods and specific parameters of the carrier tape and deposited layers depend on the technology [1].

As tensile tests of HTS-2G wires with carrier tapes made of Hastelloy C-276 and Ni−W [2,3] alloys show that the electromechanical stability of the wire depends not only on the mechanical properties of the carrier tape, but also on the internal residual stress in the superconducting layer. Being compressive, it to some extent compensates for the external tensile stress and thus prevents the layer destruction. The results of studying the electromechanical properties of thin-layer HTS-2G wires with carrier tape made of stainless steel AISI 310S [4] lead to the same conclusion. Taking into account the epitaxial relation between the superconducting and buffer layers, it can be assumed that the residual stresses in the buffer layers act in a similar way. The real significance of residual stresses for the electromechanical stability of HTS-2G wires can only be established experimentally as a result of direct measurements.

Residual stresses inside the AISI 310S carrier tape at the initial stages of wire fabrication were measured using neutron stress diffractometry [5,6]. The stresses in the superconducting and buffer layers can only be determined by x-ray methods [7]. Such studies are carried out on REBCO and YBCO superconducting layers grown on $LaAlO_3$ and $SrTiO_3$ single-crystal substrates [8–11]. In terms of technology, these layers have little in common with real layers in HTS-2G wires, so the results obtained should be treated critically. Residual stress in real buffer layer YSZ (ZrO_2, stabilized Y_2O_3, Yttria Stabilized Zirconia) on Hastelloy tape was measured in [12]. But the result, as it turned out, is not applicable to other tapes. In particular, in terms of the total balance of elastic forces, it does not agree with the data on the residual stress inside the AISI 310S tape

Table 1. Elemental composition and linear absorption coefficients of CuK_α-radiation μ for AISI 310S stainless steel tape and YSZ layer (error in last character in brackets)

	Composition								Density, g/cm^3	μ, cm^{-1}
Tape AISI 310S	wt.%								7.9	1853.6
	Ni	Cr	Fe	Mn	C	P	S	Si		
	20.3(2)	24.1(3)	54.4(2)	1.28(2)	0.25	0.045	0.030	1.50		
Layer YSZ	$Y_xZr_{1-x}O_2$ $x = 0.146(2)$				Content Y_2O_3, mol.% 7.9(1)				6.0	625.3

with the same layer [6]. Obviously, in each HTS-2G wire, the residual stresses are individual, and they can be reliably determined only during the wire manufacturing process.

Previously [5,6] we measured the residual stresses inside the AISI 310S tape used as a carrier in the manufacture of HTS-2G wires at Research Center „Kurchatov Institute", from delivery to deposition of the main YSZ buffer layer inclusively. Here we present the results of X-ray diffraction study of residual stresses on the surface of this tape at the same stages of wire fabrication, as well as in the YSZ buffer layer itself. The study was performed on the units of the Resource Center „Rentgen" of Research Center „Kurchatov Institute" [13].

1. Methodological part

1.1. Samples

As samples the same tapes, on which neutron studies were carried out [5,6], were used to ensure the continuity of the results.

(1) AISI 310S original stainless steel tape 100 μm thick and 4 mm wide as delivered by the mill, cold-rolled semi-work-hardened, tensile strength, according to the standard, $\sigma_B = 600-750$ MPa.

(2) Polished tape — original tape, one of the sides of which was subjected to mechanical polishing at room temperature using aluminum oxide as an abrasive with a particle size of 1 and 0.3 μm; the thickness of the polished tape is about 98 μm.

(3) Tape with a textured yttrium-stabilized zirconia (YSZ) buffer layer deposited to the polished side using ABAD (Alternating Beam Assisted Deposition) [14] at 50°C. The thickness of the YSZ layer, determined using the NanoCalc-VIS Ocean Optics system for thin film reflectometry, is 2.1 μm.

The elemental composition of the AISI 310S tape and the YSZ layer is given in Table 1; the linear absorption coefficients of CuK_α radiation, which was used in the work, are also given there. The composition was determined as a result of X-ray microfluorescence analysis on Bruker AXS M4 TORNADO spectrometer by ten points uniformly distributed over the width of the tape at length of 10 mm; for light elements (C, Si, P and S) the data are taken from [15]. Absorption coefficients are calculated according to Tables [16]; the calculations used the density of a single crystal 8 mol.% $Y_2O_3-ZrO_2$ [17], which is close in composition to the YSZ layer, and the X-ray density of the tape AISI 310S with $a_0 = 3.59$ Å [6].

The penetration depth of X-ray radiation into a flat sample, t, is estimated as [18]:

$$t = \frac{4.61}{2\mu} \sin\theta,$$

where μ and θ — linear absorption coefficient and angle of incidence/reflection of radiation onto the sample surface, respectively. For the YSZ layer the penetration depth of CuK_α radiation in the working range of angles θ from 10 to 50° is from 6 to 28 μm (see μ in Table 1), which exceeds its thickness by 3–14 times. Therefore, the measured residual stresses will be averaged over the entire thickness of the layer YSZ. The situation is different with AISI 310S tape. For it, in the same range of angles, the penetration depth of CuK_α radiation is from 2 to 10 μm, and only a thin layer on the surface will be visible in the experiment. Its thickness will be different for reflections from different crystal planes (hkl), and each reflection will carry information about the layer in which it was formed.

The quantitative determination of residual stresses in a material requires knowledge of its unstressed state. For thin layers, such information is not always available. Although methods were developed that make it possible to work without it [19], the reliability of the results obtained with their help often raises questions. Therefore, the unstressed state of the YSZ layer was obtained experimentally. For this purpose, the YSZ layer was deposited on the unpolished surface of the steel tape under the same conditions as on the polished one. Then the tape was quickly, within a few seconds, heated to about 400°C, after which the layer flaked off (note that higher heating to 800°C does not lead to this effect).

To assess the unstressed state of the steel tape, AISI 310S cold-rolled tape without cold-hardening, with tensile strength of $\sigma_B = 520-550$ MPa was used.

1.2. Determination of residual stresses

Residual elastic stresses in thin layers are determined by the deformation caused by them — change in distances d between crystal planes (hkl) [19] (Fig. 1). Interplanar spacings are measured by X-ray diffraction using the Wulff–Bragg law

$$2d\sin\theta = \lambda n,$$

where λ — radiation wavelength, θ — Bragg angle of reflection, n — order of reflection, measurements are made for first-order reflections, $n = 1$. In the general case, stress and strain are anisotropic and depend on the direction in the layer plane (angle ξ in Fig. 1). But for the tapes under study, they can be considered isotropic [6].

Under isotropic stress and strain for a polycrystalline layer

$$\varepsilon_\psi = \frac{d_\psi - d_0}{d_0} = \sigma\left(-\frac{2\nu}{E} + \frac{1+\nu}{E}\sin^2\psi\right), \qquad (1)$$

where d_0 and d_ψ — interplanar distances for the unstressed and stressed states, respectively, ε_ψ and σ — relative strain and the average stress in the layer, respectively, ψ — the angle between the scattering vector and the normal to the layer surface (Fig. 1), E and ν — Young's modulus and Poisson's ratio, respectively. For AISI 310S steel $E = 200$ GPa and $\nu = 0.27$ [20].

If the layer is single-crystal, then the strain and stress in it are determined by elastic constants. For a cubic single crystal, which is 8 mol.% Y_2O_3–ZrO_2 [17], the number of independent elastic stiffness constants c and associated with them elastic compliance constants s is three — c_{11}, c_{12}, c_{44} and s_{11}, s_{12}, s_{44} [19,21]. And if the interface between the layer and the substrate is (001), as in the case of YSZ [12], then

$$\varepsilon_\psi = \frac{d_\psi - d_0}{d_0} = \sigma\left[2s_{12} + (s_{11} - s_{12})\sin^2\psi\right], \qquad (2)$$

where

$$s_{11} = \frac{c_{11} + c_{12}}{(c_{11} - c_{12})(c_{11} + 2c_{12})},$$

$$s_{12} = \frac{-c_{12}}{(c_{11} - c_{12})(c_{11} + 2c_{12})}, \quad s_{44} = \frac{1}{c_{44}}. \qquad (3)$$

From the elastic constants of single crystal, one can calculate common for polycrystalline materials bulk modulus K, Young's modulus E, and Poisson's ratio ν [22,23]:

$$K = \frac{c_{11} + 2c_{12}}{3}, \; E_i = \frac{9KG_i^*}{3K + G_i^*}, \; \nu_i = \frac{3K - 2G_i^*}{2(3K + G_i^*)}, \qquad (4)$$

where

$$G_1^* = G_1 + 3\left(\frac{5}{G_2 - G_1} - 4\beta_1\right)^{-1},$$

$$G_2^* = G_2 + 2\left(\frac{5}{G_1 - G_2} - 6\beta_2\right)^{-1}, \qquad (5)$$

$$G_1 = \frac{c_{11} - c_{12}}{2}, \quad G_2 = c_{44},$$

$$\beta_1 = -\frac{3(K + 2G_1)}{5G_1(3K + 4G_1)}, \quad \beta_2 = -\frac{3(K + 2G_2)}{5G_2(3K + 4G_2)}.$$

The index $i = 1, 2$ in formulas (4) refers to the stiffnesses G_1^* and G_2^* (5), the largest of which is the Hashin stiffness G_H, while the smaller — Shtrikman stiffness G_S [22].

Table 2 for a single crystal 8 mol.% Y_2O_3–ZrO_2 shows the measured values of the elastic stiffness constants [24–29] and elastic compliance constants calculated by the formulas (3). For a polycrystal of the same composition, the measured values of Young's modulus E_{exp} and Poisson's ratio ν_{exp} [30] are also given in comparison with the upper and lower boundaries defined by formulas (4) and (5).

In single-crystal layers, due to the narrow range of angles ψ available for measurements on one crystal plane, residual stresses are determined by the CGM (Crystallite Group Method) method, using several planes from different crystal groups $\{hkl\}$ [31–33]. If the problem conditions allow, then it is sufficient to use the planes of one crystalline zone, which contains a crystalline plane parallel to the layer surface ($\psi = 0$). The sample is rotated around the zone axis by angles ψ corresponding to the angles between the zone planes, and the interplanar distances d_ψ for these planes are measured [33]. The relative strain for the zone planes is calculated as usual: $\varepsilon_\psi = (d_\psi - d_0)/d_0$. As a result, the deformation in the single-crystal layer becomes known in a wide range of angles ψ, which is given by the angles between the planes of the zone.

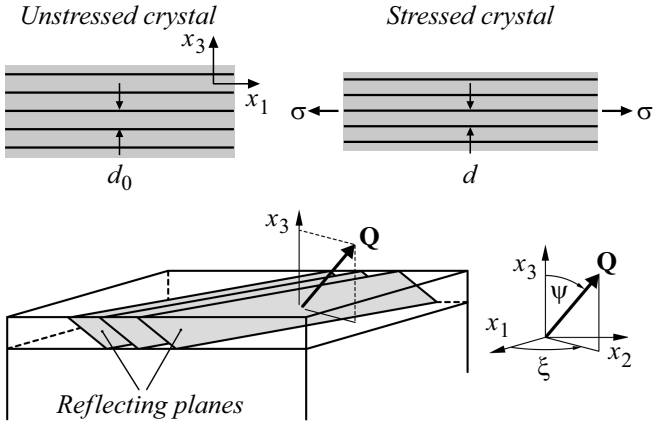

Figure 1. On determination of residual elastic stresses in thin crystalline layers [19] (explanations in text). Top — schematic representation of distances d_0 between crystal planes (hkl) in an unstressed crystal (left) and distances d in the same crystal subjected to equi-biaxial tensile stress σ (right). Below — schematic representation of reflecting crystal planes in a layer on substrate. The planes are oriented so that the X-ray scattering vector Q $(= 2\pi/d)$ perpendicular to them forms an angle ψ with the normal to the layer surface (axis x_3), and the projection Q to this surface (x_1, x_2) forms angle ξ with the x_1 axis.

Table 2. Elastic stiffness constants c and elastic compliance constants s calculated by formula (3) for a cubic single crystal 8 mol.% $Y_2O_3-ZrO_2$. Young's modulus E_{exp}, Poisson's ratio ν_{exp} and their boundary values E_H, E_S and ν_H, ν_S calculated by formulas (4) and (5) for polycrystal

c_{11}, GPa	c_{12}, GPa	c_{44}, GPa	Reference
394.0	91.0	56.0	[24,25,26]
410.0	90.0	53.0	[24,27]
415.0	119.0	57.0	[24,27]
408.2	82.4	54.0	[28]
401.8	95.2	55.8	[29]
405.8	95.5	55.2	Average value
8.1	13.9	1.6	Standard deviation
s_{11}, GPa^{-1}	s_{12}, GPa^{-1}	s_{44}, GPa^{-1}	
0.00271 ± 0.00007	-0.00052 ± 0.00007	0.01814 ± 0.00054	
E_{exp}, GPa [30]	E_H, GPa	E_S, GPa	
221.0 ± 1.4	225.9 ± 1.5	216.0 ± 2.4	
ν_{exp} [30]	ν_H	ν_S	
0.320 ± 0.001	0.310 ± 0.009	0.319 ± 0.008	

1.3. Measurements

The measurements were carried out using CuK_α radiation on powder diffractometer Bruker D8 Advance and four-circle diffractometer Rigaku SmartLab, at room temperature. To refine the positions of the diffraction peaks, an internal standard Ge was used, which was deposited on the surface of the samples in the form of a finely dispersed powder. The data obtained were processed by full profile analysis using the software package FullProf Suite [34]. The diffraction peak profiles were fitted using K_α doublet with overlapping pseudo-Voigt shape components. Interplanar distances d were determined from the center of gravity of the peaks.

The data for the steel tape were obtained at $\psi = 0$ on reflecting planes parallel to the rolling plane. The YSZ layer was measured in the same geometry on the plane (002) parallel to the layer surface. Data verification was carried out using the CGM method with a point focus of 100 μm. The crystal zone [$\bar{1}$10] with the axis transverse to the tape rolling direction and (002), (113), (111) and (331) planes was used (insert in Fig. 2). In the cubic cell the angles ψ for these planes are 0, 25.24, 54.74 and 76.74°, respectively.

The data for the unstressed state of YSZ were obtained on flakes of the layer peeled from the unpolished tape. The data for the unstressed state of the AISI 310S tape were obtained on the tape without cold-hardening.

2. Results

2.1. Layer YSZ

Fig. 2 shows the X-ray diffraction pattern and the pole figure from the {111} planes for the YSZ layer on the tape in comparison with the X-ray diffraction pattern for the free YSZ layer in the unstressed state. The YSZ layer on the tape has a pronounced biaxial texture [110] (002) with scatter less than 10°: two axes of the cubic cell lie in the tape plane at angles of 45° to the rolling direction, the third axis is perpendicular to the plane of the tape (insert in Fig. 2). The diffraction peaks from the steel tape are clearly visible through the YSZ layer. Attention is drawn to the large width of reflections (002) and (004), which is eight times greater than the width of the peaks from the steel tape. In the free layer YSZ

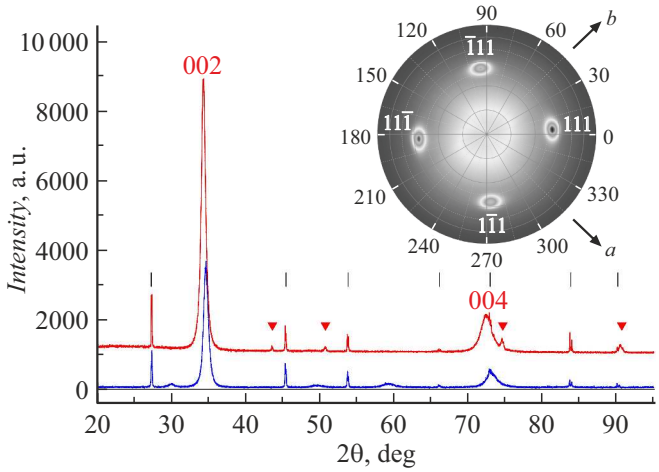

Figure 2. Diffraction pattern from the YSZ layer on the tape (top) and in unstressed state (bottom). The peaks from the steel tape are marked with triangles, the peaks from Ge — vertical lines. In the insert — the pole figure from the {111} planes, the zero angle corresponds to the steel tape rolling direction, the arrows show the directions of the a and b axes of the YSZ cell.

the width of the reflections does not change, and the reflections themselves shift to larger angles; the interplanar distance (002) decreases from 2.61525(5) to 2.59101(8) Å. This means that the YSZ layer on the tape is compressed. Compression stress calculated by formulas (1) and (2) at $\psi = 0$ and data from Table 2 is -3.29 ± 0.18 GPa for polycrystal and -8.99 ± 1.26 GPa for a single crystal. A similar result is obtained by the CGM method (Fig. 3). The experimental points ε_ψ are well approximated by the linear in $\sin^2\psi$ function $\varepsilon_\psi = 0.0094 - 0.0218\sin^2\psi$. The compression stress calculated by the slope of the straight line is -3.66 ± 0.33 GPa for a polycrystal, which, within the error, agrees with the value obtained at $\psi = 0$. For a single crystal it is somewhat less than at $\psi = 0$, -6.75 ± 0.61 GPa (obviously, due to the use of different elastic constants in the calculations), but still much larger than for the polycrystal. This fact has a simple explanation.

In the free YSZ layer the cubic cell parameter is 5.18202 ± 0.00016 Å, which is by 0.9% larger than the cell parameter of the ordinary single crystal of the same composition, 5.135 ± 0.005 Å [17]. At the same time, a large reflection width indicates the presence of strong microstresses in the structure (caused by dislocations, slip plane defects, static displacements of atoms from lattice sites, etc. [35]). In other words, the YSZ layer has a swollen defective crystalline structure, which is not surprising if we take into account the strong nonequilibrium conditions for its formation — under the action of an intense flow of high-energy ions Ar [14]. This effect, similar to the radiation swelling of the material, requires a separate study. However, it is already clear that, compared

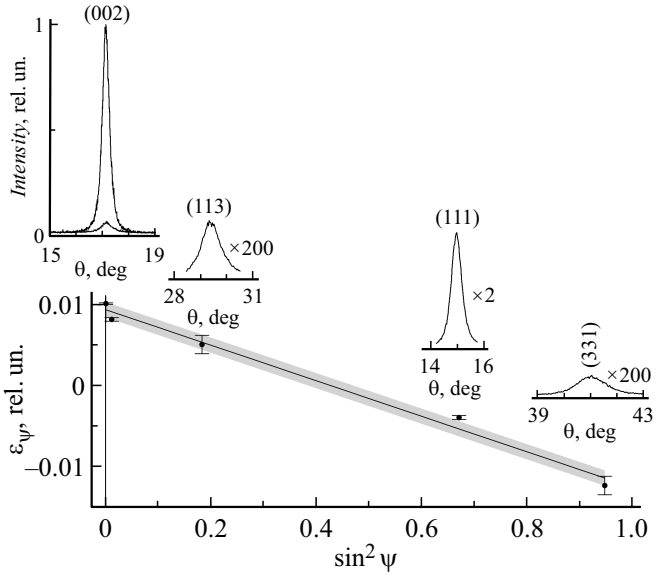

Figure 3. Dependence on $\sin^2\psi$ of deformation ε_ψ for the planes (002), (113), (111) and (331) of the crystal zone $[1\bar{1}0]$ in the layer YSZ on the tape. The area within the mean square deviation from the linear approximation (solid line) is indicated in gray color. The profile of the Bragg peak is shown for each plane, for (002) at $\psi = 0$ and 6°.

with a conventional single crystal, the density of the YSZ layer is significantly reduced (almost by 3%), hence its rigidity is reduced. Therefore, the calculation of the internal stress by single-crystal data gives an overestimated result.

As for the value obtained for the polycrystal, -3.29 ± 0.18 GPa, in terms of the total balance of elastic forces it ideally corresponds to the average stress in the steel tape-substrate +70 MPa, determined by the neutron method [6]:

$$-3.29\,\text{GPa} \times 2.1\,\mu\text{m} + 70\,\text{MPa} \times 98\,\mu\text{m} \approx 0. \qquad (6)$$

2.2. Tape AISI 310S

Diffraction patterns from the AISI 310S tape at different stages of tape processing are shown in Fig. 4. The interplanar distances d determined from them for the planes (hkl) are shown as the parameter $a_d = d\sqrt{h^2 + k^2 + l^2}$ in Fig. 5, left. The lattice period for tape without cold-hardening (extrapolated to $\theta = 90°$) is 3.5939 ± 0.0001 Å and almost coincides with the value 3.5936 ± 0.0002 Åfound for an unstressed state in neutron research [6]. Relative strain ε_{310S} and stress σ_{310S} determined by formula (1) at $\psi = 0$ are given in Fig. 5, right.

According to the data obtained, the following changes occur on the surface of the tape during processing. Initially, the tape surface is compressed, and there is compression stress -0.8 GPa caused by rolling, which extends deeper by more than $10\,\mu$m (Fig. 5, bottom right). During mechanical polishing (Fig. 6, top left) compression increases on the polished side and decreases on the unpolished side by approximately the same value, about 0.3 GPa. The effect quickly disappears with depth (on the polished side already at $10\,\mu$m) and has a simple explanation. Surface polishing causes plastic deformation at a shallow depth and, as a result, additional compression of the polished side; to compensate for it, the opposite side is slightly tensioned. After applying the YSZ layer (Fig. 6, bottom left), the compression stress on the polished side, under the YSZ layer, noticeably decreases — by 0.4 GPa, and becomes only weaker with depth. On the opposite side, it, on the contrary, intensifies, and this side of the tape almost returns to its initial state (the difference of 40 MPa is at the level of error). In other words, under the YSZ layer the tape is stretched, and the tension extends deep into the tape; to compensate this the opposite side of the tape is compressed. Note that during processing the surface of the tape always remains compressed, the stress on it varies from -0.5 to -1.1 GPa. The residual stresses introduced at each stage can be visualized as difference of the stresses before and after processing (Fig. 6, right).

A few words about stresses under the YSZ layer. Previously [6], based on residual stress data in the YSZ layer on Hastelloy tape (-365 MPa [12]) and the need to

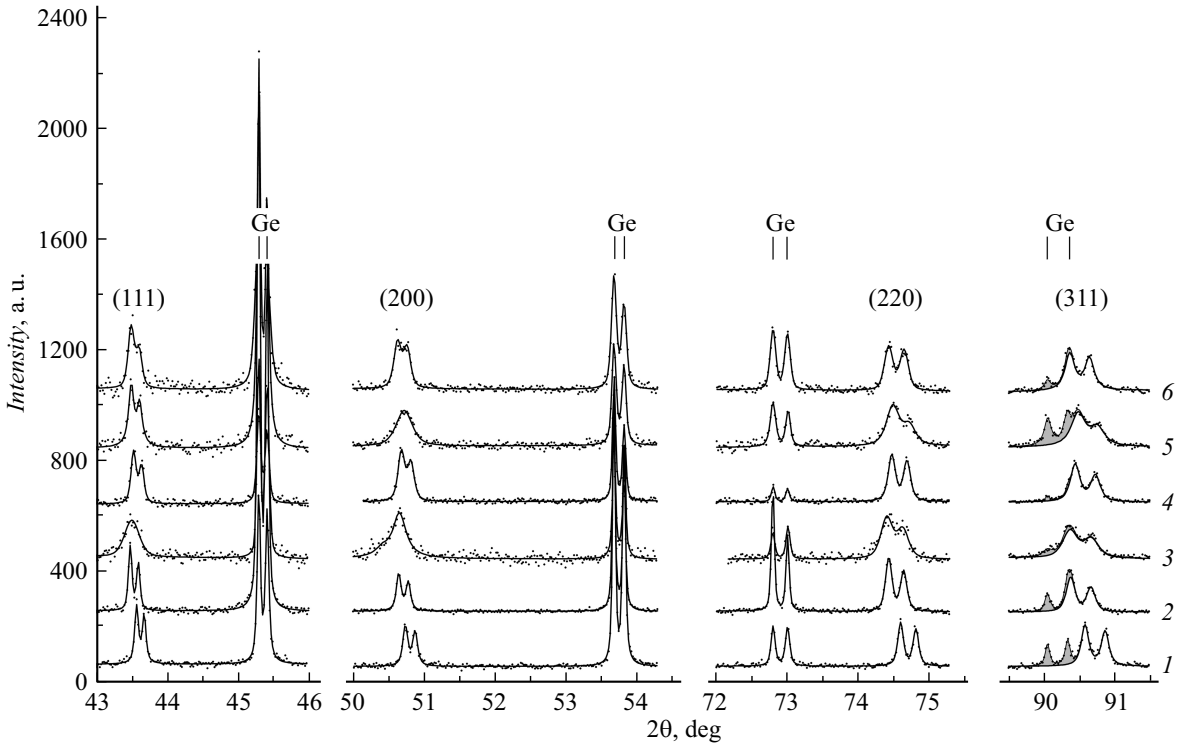

Figure 4. Diffraction peaks from planes (*hkl*) of the AISI 310S tape and reference peaks of Ge (for (311) shaded), dots — experiment, lines – - fitted profile. *1* — tape without cold-hardening, *2* — original tape as delivered, *3* — polished side of the original tape after mechanical polishing, *4* - – unpolished side, *5* — surface under the YSZ layer (cf. Fig. 2), *6* — opposite side free from YSZ layer.

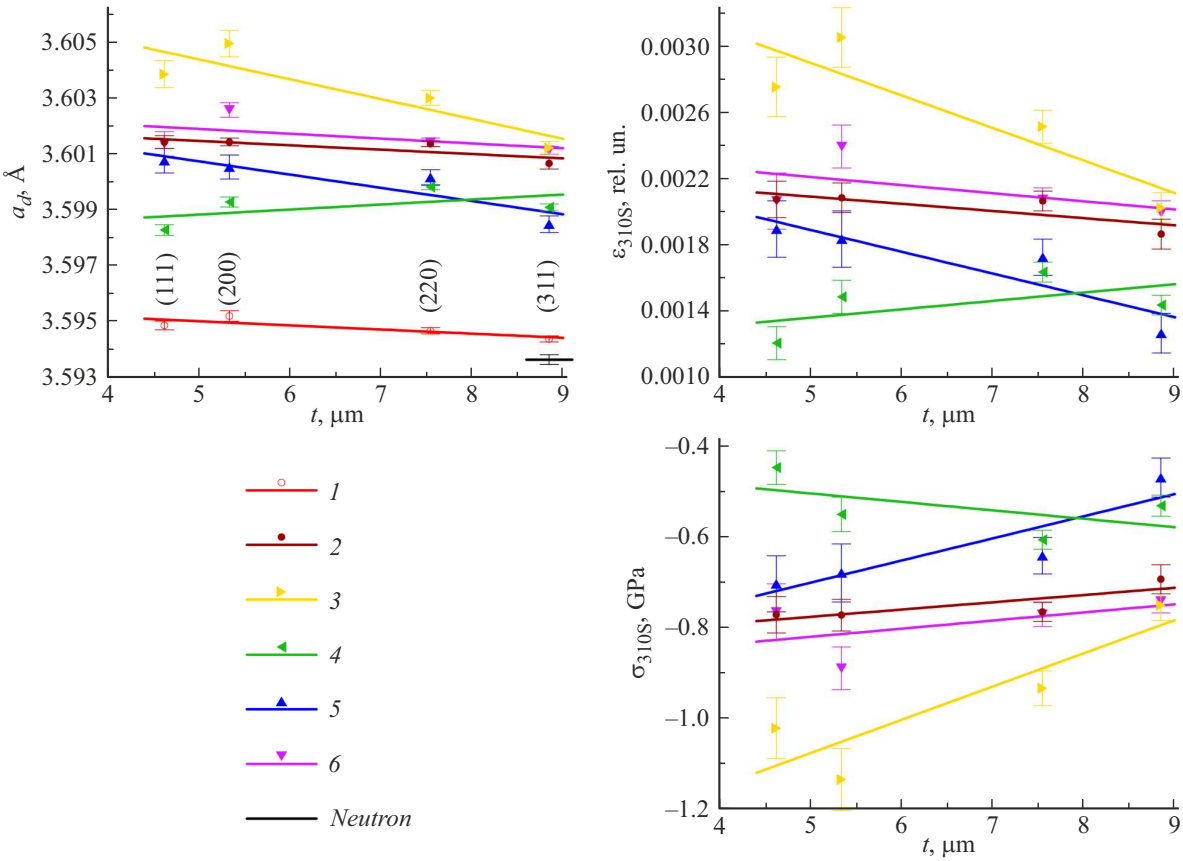

Figure 5. Left — change with layer thickness t of parameter $a_d = d\sqrt{h^2 + k^2 + l^2}$ on the surface of the AISI 310S tape. Designations, as in Fig. 4, additionally show the lattice period for the unstressed state, found by the peak (311) in the neutron study [6]. On the right — relative strain ε_{310S} (top) and stress σ_{310S} (bottom), calculated by formula (1) at $\psi = 0$.

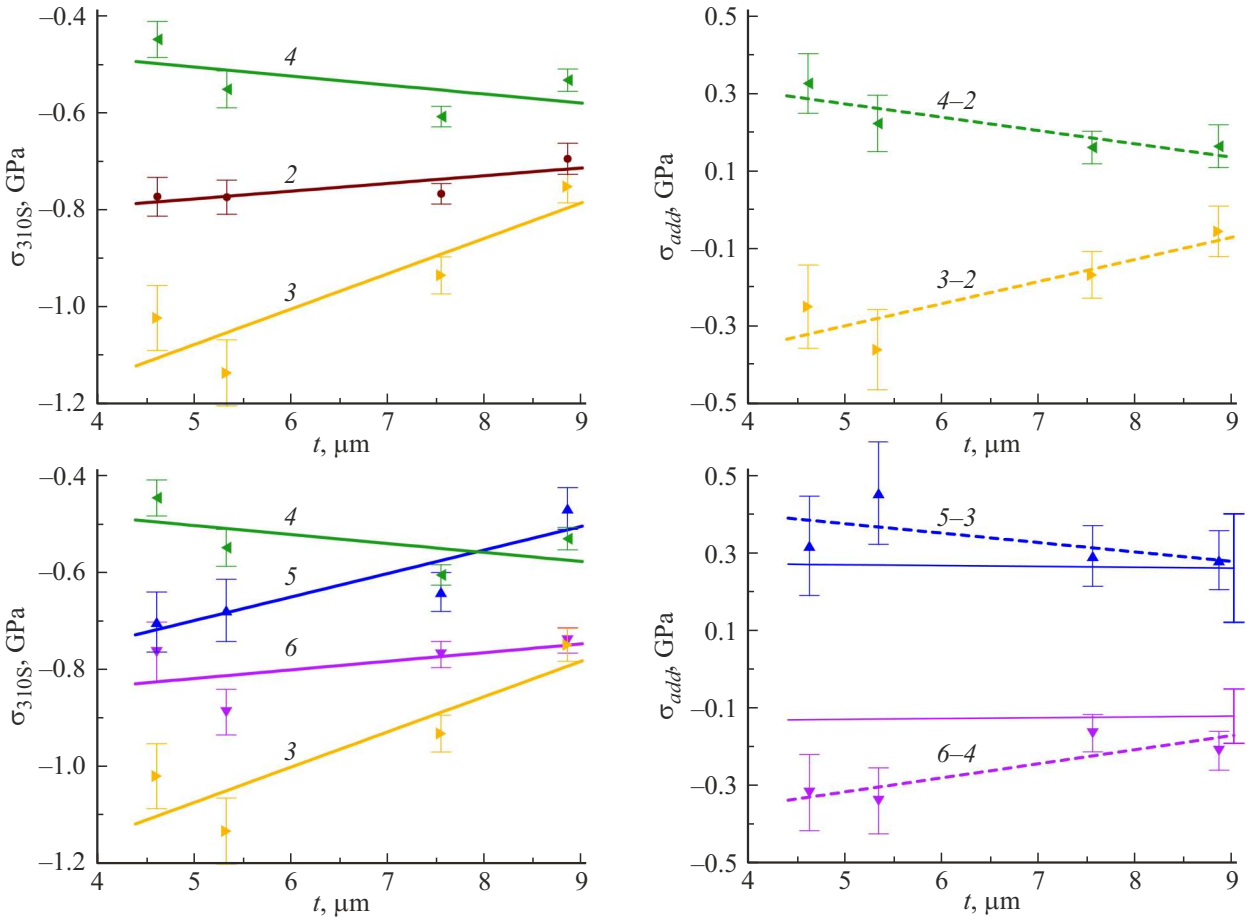

Figure 6. Left — change with layer thickness t of residual stress σ_{310S} on the surface of AISI 310S tape during mechanical polishing (top) and subsequent deposition of YSZ layer (bottom), designations as in Fig. 5. Right — σ_{add} stresses (dashed lines) introduced by mechanical polishing (top) and YSZ layer deposition (bottom), as difference of stresses σ_{310S} before and after processing (indicated by numbers), thin solid lines — calculation based on neutron data [6].

maintain a total balance of elastic forces in AISI 310S tape with the same layer, an assumption was made about the possible existence of a compression stress under this layer in the AISI 310S tape. The results of the present work do not confirm this assumption. The residual stress in the YSZ layer on the AISI 310S tape is by order of magnitude greater than that in the YSZ layer on the Hastelloy tape, and the balance of forces is observed naturally (6) without additional assumptions. Moreover, the stresses induced by the YSZ layer agree satisfactorily with those expected from the neutron data (Fig. 6, right bottom).

Conclusion

Let us briefly summarize the main results of the study.

1. On the surface of the original as delivered AISI 310S tape, there is a compression stress -0.8 GPa. During mechanical polishing and depositing the YSZ layer, the tape surface remains compressed, the residual stress on it varies from -0.5 to -1.1 GPa. At each stage of processing, the distribution of residual stresses through the depth down to $10\,\mu$m was found, and the stresses introduced by processing were determined.

2. The residual stress in the YSZ layer applied by ABAD technology is compressive and amounts to -3.29 ± 0.18 GPa. The layer has a defective single-crystal structure, similar to that formed during radiation swelling, which remains the same in unstressed state. The lattice period in the unstressed state, 5.1820 Å, is by 0.9% larger than in an ordinary crystal.

3. The results of the X-ray study are in agreement with the results obtained earlier by the neutron method on the same tapes. In the tape with YSZ layer the total balance of elastic forces is observed. The residual stress induced by the YSZ layer on the tape surface coincides with the stress calculated from the neutron data.

4. The technique used in the work, which provides for the need to coordinate data for different wire components, seems promising for a reliable determination of residual stresses in real HTS-2G wires.

Funding

The work was carried out with the financial support of the Ministry of Science and Higher Education of the Russian Federation under the agreement on the provision of grants from the federal budget in the form of subsidies dated December 22, 2021 №075-11-2021-086 (government contract ID №000000S507521RN60002).

Conflict of interest

The authors declare that they have no conflict of interest.

References

[1] J.L. MacManus-Driscoll, S.C. Wimbush. Nat. Rev. Mater., **6**, 587 (2021). DOI: 10.1038/s41578-021-00290-3
[2] K. Osamura, M. Sugano, S. Machiya, H. Adachi, M. Sato, S. Ochiai, A. Otto. Supercond. Sci. Technol., **20**, S211 (2007). DOI: 10.1088/0953-2048/20/9/S15
[3] K. Osamura, M. Sugano, S. Machiya, H. Adachi, S. Ochiai, M. Sato. Supercond. Sci. Technol., **22**, 065001 (2009). DOI: 10.1088/0953-2048/22/6/065001
[4] A. Krivykh, A. Irodova, V. Krylov, I. Kulikov, A. Polyakov. IEEE Trans. Appl. Supercond., **32** (4), 8400105 (2022). DOI: 10.1109/TASC.2022.3143773
[5] I.D. Karpov, A.V. Irodova, V.S. Kruglov, S.V. Shavkin, V.T. Em. Tech. Phys., **65** (7), 1051 (2020). DOI: 10.1134/S1063784220070063
[6] A.V. Irodova, I.D. Karpov, V.S. Kruglov, V.E. Krylov, S.V. Shavkin, V.T. Em. ZhTF, **91** (12), 1966 (2021) (in Russian). DOI: 10.21883/JTF.2021.12.51761.169-21
[7] U. Welzel, J. Ligot, P. Lamparter, A.C. Vermeulen, E.J. Mittemeijer. J. Appl. Crystallogr., **38**, 1 (2005). DOI: 10.1107/S0021889804029516
[8] J. Xiong, W. Qin, X. Cui, B. Tao, J. Tang, Y. Li. Physica C Supercond., **455**, 52 (2007). DOI: 10.1016/J.PHYSC.2007.02.006
[9] F. Li, S. Wang, Z. Zhang, S. Muhammad, X. Le, Z. Xiao, X. Ouyang. Physica C Supercond., **564**, 68 (2019). DOI: 10.1016/J.PHYSC.2019.06.008
[10] J. Yu, F. Li, J.-B. Fan, S. Muhammad, Y.P. Dahal, Z. Zhang, S. Wang. Physica C Supercond., **577**, 1353728 (2020). DOI: 10.1016/j.physc.2020.1353728
[11] S. Favre, D. Ariosa, C. Yelpo, M. Mazini, R. Faccio. Mater. Chem. Phys., **266**, 124507 (2021). DOI: 10.1016/j.matchemphys.2021.124507
[12] J.H. Cheon, P.S. Shankar, J.P. Singh. Supercond. Sci. Technol., **18**, 142 (2005). DOI: 10.1088/0953-2048/18/1/022
[13] Resursny tsentr laboratornykh rentgenovskikh metodov „Rentgen" (in Russian) URL: http://www.rc.nrcki.ru/pages/main/rentgen/index.shtml
[14] A. Usoskin, L. Kirchhoff. Mater. Res. Soc. Symp. Proc., **1150**, 1150-RR05-02 (2009). DOI: 10.1557/PROC-1150-RR05-02
[15] K.J. Radcliff, R.P. Walsh, D.C. Larbalestier, S. Hahn. IOP Conf. Series: Materials Science and Engineering, **756**, 012023 (2020). DOI: 10.1088/1757-899X/756/1/012023
[16] *International Tables for Crystallography, Volume C: Mathematical, Physical and Chemical Tables* (Kluwer Academic Publishers, Dordrecht, 2004), DOI: 10.1107/97809553602060000103
[17] R.P. Ingel, D. Lewis. J. Am. Ceram. Soc., **69** (4), 325 (1986). DOI: 10.1111/j.1151-2916.1986.tb04741.x
[18] T. Mitsunaga. The Rigaku J., **25** (1), 7 (2009)
[19] L.B. Freund, S. Suresh. *Thin Film Materials. Stress, Defect Formation and Surface Evolution* (Cambridge University Press, NY., 2004), DOI: 10.1017/CBO9780511754715.003
[20] AISI 310S (S31008) Stainless Steel. URL: https://www.makeitfrom.com/material-properties/AISI-310S-S31008-Stainless-Steel
[21] *International Tables for Crystallography, Volume D: Physical properties of crystals* (Kluwer Academic Publishers, Dordrecht, 2003), DOI: 10.1107/97809553602060000113
[22] G. Simmons, H.F. Wang. *Single Crystal Elastic Constants and Calculated Aggregate Properties. A Handbook* (MIT Press, Cambridge, 1971)
[23] R. Hill. Proceed. Phys. Society, Section A, **65** (5), 349 (1952). DOI: 10.1088/0370-1298/65/5/307
[24] R.P. Ingel, D. Lewis. J. Am. Ceram. Soc., **71** (4), 265 (1988). DOI: 10.1111/J.1151-2916.1988.TB05858.X
[25] N.G. Pace, G.A. Saunders, Z. Sumengen, J.S. Thorp. J. Mater. Sci., **4**, 1106 (1969). DOI: 10.1007/BF00549851
[26] J.M. Farley, J.S. Thorp, J.S. Ross, G.A. Saunders. J. Mater. Sci., **7**, 475 (1972). DOI: 10.1007/BF00553773
[27] I.L. Chistyi, I.L. Fabelinskii, V.F. Kitaeva, V.V. Osiko, Y.V. Pisarevskii, I.M. Sil'vestrova. J. Raman Spectrosc., **6** (4), 183 (1977). DOI: 10.1002/jrs.1250060406
[28] M. Hayakawa, H. Miyauchi, A. Ikegami, M. Nishida. Mater. Trans. JIM, **39** (2), 268 (1998). DOI: 10.2320/MATERTRANS1989.39.268
[29] H.M. Kandil, J. Greiner, J. Smith. J. Am. Ceram. Soc., **67** (5), 341 (1984). DOI: 10.1111/J.1151-2916.1984.TB19534.X
[30] A. Selcuk, A. Atkinson. J. Eur. Ceram. Soc., **17** (12), 1523 (1997). DOI: 10.1016/S0955-2219(96)00247-6
[31] R. Kuzel, R. Cerny, V. Valvoda, M. Blomberg, M. Merisalo. Thin Solid Films, **247** (1), 64 (1994). DOI: 10.1016/0040-6090(94)90477-4
[32] B.H. Hwang, S.Y. Chiou. Thin Solid Films, **304** (1–2), 286 (1997). DOI: 10.1016/S0040-6090(97)00106-5
[33] L. Meda, K.H. Dahmen, S. Hayek, H. Garmestani. J. Cryst. Growth, **263**, 185 (2004). DOI:10.1016/j.jcrysgro.2003.10.055
[34] FullProf Suite. Crystallographic tools for Rietveld, profile matching & integrated intensity refinements of X-Ray and/or neutron data. [Electronic resource] URL: https://www.ill.eu/sites/fullprof/index.html
[35] P.J. Withers, H.K.D.H. Bhadeshia. J. Mater. Sci. Technol., **17**, 355 (2001). DOI: 10.1179/026708301101509980